3D Thermo-hygro-mechanical model for concrete

J. Ožbolt, G. Periškić & H.W. Reinhardt
Institute of Construction Materials, University of Stuttgart, Germany

ABSTRACT: In the present paper a transient three-dimensional thermo-hygro-mechanical model for concrete is presented. For a given boundary conditions the distribution of moisture, pore pressure, temperature, stresses and strains is calculated by employing a three-dimensional transient finite element analysis. The model accounts for the interaction between hygro and thermal properties of the material. These properties are coupled with the mechanical properties of concrete, i.e. it is assumed that the mechanical properties (damage) have an effect on the distribution of moisture, pore pressure and temperature. The mechanical strain, which is due to loading, temperature induced stresses and pore pressure, is calculated by employing temperature dependent microplane model for concrete. To better understand spalling of concrete cover, a preliminary 3D finite element analysis of a concrete slab exposed to high temperature is carried out. It is shown that relatively high pore pressure together with local instabilities (geometrical non-linearity) can cause spalling of concrete cover.

1 INTRODUCTION

When temperature increases for a couple of hundred of degrees Celsius, behaviour of concrete changes significantly. The concrete mechanical properties, such as strength, elasticity modulus and fracture energy, are at high temperatures rather different than for the concrete at normal temperature. At high temperature large temperature gradients lead in concrete structures to temperature-induced stresses, which cause damage. Furthermore, creep and relaxation of concrete that is due to high temperature play also an important role. The main reason for the complexity of the behaviour of concrete at high temperature is due to the fact that concrete contains water, which at high temperature changes its aggregate state and can generate significant pore pressure. Moreover, at high temperature the aggregate can change its structure or it can loose its weight through the emission of CO_2, such as calcium based stones. Although the behaviour of concrete at high temperature is in the literature well documented (Bažant and Kaplan 1996; Khoury et al. 1985a; Schneider 1986, 1988; Thelandersson 1983) further experimental and theoretical studies are needed to clarify the interaction between hygro-thermal and mechanical properties, such as for instance explosive type of failure due to spalling of concrete cover.

The main problem in the experimental investigations is due to the fact that such experiments are rather demanding, i.e. one has to perform loading and measurement at extremely high temperatures. Furthermore, such experiments can be carried out only on relatively small structures. To better understand behaviour of concrete structures, as an alternative to the experiments one can employ numerical analysis. However, one needs models, which can realistically predict behaviour of concrete at high temperature.

There are principally two groups of phenomenological models: (i) Thermo-mechanical models and (ii) Thermo-hydro-mechanical models (Gawin et al. 1999; Pearce et al. 2003; Stabler 2000; Terro 1998). In the first group of the models the mechanical properties of concrete are temperature (moisture) dependent whereas the temperature (moisture) distribution is independent of the mechanical properties of concrete. The second group of the models are from the physical point of view more realistic. Namely, in these models the physical processes that take place in concrete are coupled, i.e. the interaction between mechanical properties, temperature, moisture, pore pressure and hydration of concrete is accounted for.

In the present paper a three-dimensional (3D) model that is based on the thermo-hygro-mechanical coupling between thermo (temperature), hygro

(moisture and pore pressure) and mechanical properties of concrete is discussed. The microplane model is used as a constitutive law for concrete with model parameters being made temperature dependent. The model is implemented into a three-dimensional finite element code and its performance is first compared with theoretical results known from the literature. Subsequently, the problem of spalling of concrete cover at high temperature is investigated.

The finite element analysis is incremental, i.e. it is performed through a number of loading (time) steps. For a given temperature, humidity and loading boundary conditions, in each time step moisture, pore pressure, temperature, stresses and strains are simultaneously calculated. The analysis is based on the implicit iterative scheme.

2. THERMO-HYGRO-MECHANICAL MODEL

The present phenomenological model for concrete is thermo-hygro-mechanical model. The model is formulated in the framework of continuum mechanics under the assumption of validity of irreversible thermodynamic. The response of the model is controlled by the following unknown variables: temperature, pore pressure (moisture), stresses and strains. In the numerical model temperature, moisture and pore pressure are coupled with stress and strain, i.e. thermo-hygro part of the model depends on damage of concrete. Moreover, the relevant mechanical properties of concrete (Young's modulus, tensile strength, compressive strength and fracture energy) are temperature dependent.

2.1 *Coupled heat and moisture transfer in concrete*

The general approach for the solution of the problem of coupled heat and mass transfer in a porous solid such as concrete is within the framework of irreversible thermodynamic well known. However, there is a number of complex detail and, therefore, for the practical application the problem must be simplified (Bažant and Thonguthai 1978).

Assuming for a moment that the moisture flux ($\boldsymbol{J}$) and heat flux ($\boldsymbol{q}$) in concrete are independent of the stress and strain, the two following is valid (Bažant and Thonguthai 1978):

$$\boldsymbol{J} = -a_{Tw}\,\mathrm{grad}\,w - a_{TT}\,\mathrm{grad}\,T \tag{1a}$$

$$\boldsymbol{q} = -a_{ww}\,\mathrm{grad}\,w - a_{wT}\,\mathrm{grad}\,T \tag{1b}$$

where a_{ww}, a_{TT}, a_{wT} and a_{Tw} are coefficients, which depend on moister content w and temperature T. Moister content w is a function of T and pore pressure p. Assuming that a_{wT} and a_{Tw} are relatively small and replacing w with p, Equation 1 can be rewritten as:

$$\boldsymbol{J} = -\frac{a}{g}\,\mathrm{grad}\,p \tag{2a}$$

$$\boldsymbol{q} = -b\,\mathrm{grad}\,T \tag{2b}$$

in which b = heat conductivity, a = permeability and g = gravity constant.

Using the condition of conservation of mass, Equation 2a can be rewritten as:

$$\frac{\partial w}{\partial t} = -\mathrm{div}\,\boldsymbol{J} + \frac{\partial w_d}{\partial t} \tag{3}$$

where t = time and w_d = total mass of water released into the pore by dehydration. In the present model dehydration is not accounted for. The balance of heat together with Equation 2b requires:

$$c\rho\frac{\partial T}{\partial t} - C_a\frac{\partial w}{\partial t} - C_w\frac{\partial T}{\partial t}\boldsymbol{J}\,\mathrm{grad}\,T + w = -\mathrm{div}\,\boldsymbol{q} \tag{4}$$

where ρ, C = mass density and isobaric heat capacity of concrete, C_a = heat sorption of free water, C_w = heat capacity of water, which is in the present model neglected.

Boundary conditions at concrete surface can be defined as:

$$\mathbf{n}\cdot\boldsymbol{J} = \alpha_w(p_0 - p_E) \tag{5a}$$

$$\mathbf{n}\cdot\boldsymbol{q} = \alpha_G(T_0 - T_E) \tag{5b}$$

where α_w = surface emissivity of water, α_G = surface emissivity of heat, T_0 and p_0 are temperature and pore pressure at concrete surface and T_E and p_E are temperature and pore pressure of environmental.

2.2 *State of pore water and permeability*

The main difficulty in the above equations is determination of the material properties. Assuming no stress-dependency, the constitutive laws for p, w and T follow simplified but realistic suggestions proposed by Bažant and Thonguthai (1978). To describe the state of pore water in concrete, one has to distinguish three different states: (i) non-saturated concrete, (ii) saturated concrete and (iii) transition from non-saturated to saturated concrete. The main difficulty here is the fact that by increasing temperature the properties of concrete significantly changes. Therefore the state equations follow known theoretical background, however, in order to obtain realistic prediction the controlling parameters had to be fitted by available test data (see Bažant and Thonguthai 1978).

For non-saturated concrete ($p \le p_S$, p_S = saturation pressure) the state of pore water is described by:

$$\frac{w}{c}=\left(\frac{w_1}{c}h\right)^{1/m(T)} \quad \text{with} \quad h=\frac{p}{p_S(T)}, \quad h\le 0.96 \qquad (6a)$$

$$\text{with } m(T)=1.04-\frac{T'}{22.34+T'};\ T'=\left(\frac{T+10}{T_0+10}\right)^2 \qquad (6b)$$

where, T = temperature in °C, T_0 = 25°C, mass of cement per m^3 of concrete and w_1 = saturation water content at 25°C.

For saturated concrete one can theoretically calculate p for given w and T by using steam tables. This would, however, already for relative low temperatures yield to extremely high pore pressure, which is not realistic. Porosity of concrete n at higher temperatures increases because of dehydration and chemical changes of cement paste (Bažant and Cusatis 2005). Therefore, to account for these effects, the initial porosity of concrete n_0 must be corrected by an empirical correction function:

$$n=\left(n_0+\frac{w_{d(T)}-w_{d0}}{\rho_0}\right)P(h) \quad for \quad h\ge 1.04 \qquad (7a)$$

$$P(h)=1+0.12\left(h-1.04\right), \quad h=\frac{p}{p_S(T)} \qquad (7b)$$

Function P was identified by fitting of test data and $w_d(T)$ was taken from the measurements of weight loss of specimens of heated concrete in thermodynamic equilibrium (Harmathy & Allen 1973). Using Equations 7a and 7b, water content in saturated concrete can be calculated as:

$$w=\left(1+3\varepsilon^V\right)\frac{n}{v}$$
$$\text{with } d\varepsilon^V=\frac{d\sigma^V}{3K}+\alpha\, dT,\ \sigma^V=np \qquad (8)$$

in which ε^V = volumetric strain due to the resulting volumetric stress σ^V caused by pore pressure, K = bulk modulus and α = coefficient of linear thermal expansion of concrete.

Except for an extremely slow change in pore pressure, the transition from non-saturated to saturated concrete can be abrupt. For most practical situations the transition is most likely smooth. Furthermore, an abrupt transition would cause numerical difficulties. Therefore, for relative vapor pressure between 0.96 and 1.04, linear increase of free water content was assumed (Bažant and Thonguthai 1978).

The permeability function for concrete also follows suggestions proposed by Bažant and Thonguthai (1978). Due to the fact that porosity of concrete above 100°C increases by about two order of magnitude, a function which controls permeability consists of two parts – for $T\le 95$°C and for $T>95$°C. For more detail see Bažant and Thonguthai (1978).

2.3 *Thermo-mechanical coupling*

In the present model the total strain tensor $\boldsymbol{\varepsilon}$ for stressed concrete exposed to high temperature can be decomposed as (Khoury et al. 1985a; Schneider 1986; Thelandersson 1987):

$$\boldsymbol{\varepsilon}=\boldsymbol{\varepsilon}^m(T,\boldsymbol{\sigma})+\boldsymbol{\varepsilon}^{ft}(T)+\boldsymbol{\varepsilon}^{tm}(T,\boldsymbol{\sigma})+\boldsymbol{\varepsilon}^c(T,\boldsymbol{\sigma}) \qquad (9)$$

where $\boldsymbol{\varepsilon}^m$ = mechanical strain tensor, $\boldsymbol{\varepsilon}^{ft}$ = free thermal train tensor, $\boldsymbol{\varepsilon}^{tm}$ = thermo-mechanical strain tensor and $\boldsymbol{\varepsilon}^c$ are strains that are due to the temperature dependent creep of concrete. In the following the strain components are only briefly discussed. For more detail see (Ožbolt et al. 2005).

In general, the mechanical strain component can be decomposed into elastic, plastic and damage part. The source of this strain tensor is external load, thermal induced stress and pore pressure in concrete. In the present model these strain components are calculated using temperature dependent microplane model. The parameters of the microplane model are modified such that the macroscopic response of the model fits temperature dependent mechanical properties of concrete.

Free thermal strain is stress independent and it is experimentally obtained by measurements on a load-free specimen. In such experiments it is not possible to isolate shrinkage of concrete. Therefore, the temperature dependent shrinkage is contained in the free thermal strain.

The thermo-mechanical strain is stress and temperature dependent. It appears only during the first heating and not during the subsequent cooling and heating cycles (Khoury et al. 1985a). This strain is irrecoverable and lead in concrete structures to severe tensile stresses during cooling.

Temperature dependent creep stain is of the same nature as the thermo-mechanical strain except that it is partly recoverable. In an experiment it is not possible to isolate this strain. For low temperature rate, which is normal case in the experiments, this strain component compared to the thermo-mechanical strain is small. Therefore, temperature dependent creep stain is in the present model neglected.

2.4 *Thermo-hygro-mechanical coupling*

In the thermo-mechanical part of the model temperature is coupled with mechanical properties of concrete but only in one direction. In thermo-hygro-mechanical model, thermo-hygro process must be coupled with mechanical properties of concrete in both directions. It is known that the

porosity of concrete is a relevant parameter that controls thermo-hygro processes in concrete. On the other hand, the porosity is strongly influenced by damage, i.e. by higher level of damage the porosity is higher. Therefore, as a first approximation it is assumed that the porosity is a linear function of damage:

$$n_d = n + \left(n_{\max} - n\right) d \tag{10}$$

in which n_d = total porosity (thermo-hygro + damage contribution), $n_{\max}$ = upper porosity limit and d = damage ($0 \le d \le 1$). Note that because of numerical reasons the upper limit on porosity is not set to 1 but it is assumed to be equal to the porosity of extremely porous light-weight concrete. All thermo-hygro properties of concrete are related to the porosity n_d. Therefore, in the constitutive equations n needs to be replaced by n_d. Damage is calculated using temperature dependent microplane model (Ožbolt et al. 2001, Ožbolt et al. 2005).

3. NUMERICAL IMPLEMENTATION

The numerical analysis is incremental. In each time step Δt simultaneously are solved partial differential equations, which control heat and moisture transfer in concrete, and differential equation of equilibrium (mechanical part of the model). It is assumed that in each time step damage is constant, i.e. thermo-hygro properties of concrete are controlled by damage parameter from the end of the previous time step.

To solve the problem by the finite element method the above differential equations, which govern the heat and moisture transfer in concrete, have to be written in the weak (integral) form. After introducing the condition that the functional is stationary one obtains the following system of linear equations (Voigt notation):

$$\begin{aligned} \left[C_1\right]\left\{\dot{p}\right\} + \left[C_2\right]\left\{\dot{T}\right\} + \left[K_1\right]\left\{p\right\} &= \left\{R_1\right\} \\ \left[C_3\right]\left\{\dot{\mathrm{T}}\right\} + \left[C_4\right]\left\{\dot{p}\right\} + \left[K_2\right]\left\{\mathrm{T}\right\} &= \left\{R_2\right\} \end{aligned} \tag{11}$$

with

$$\left[C_1\right] = \int_\Omega \frac{\partial w}{\partial p}\left[N\right]^T\left[N\right] d\Omega;\ \left[C_2\right] = \int_\Omega \frac{\partial w}{\partial t}\left[N\right]^T\left[N\right] d\Omega;$$

$$\left[C_3\right] = \int_\Omega (c\rho - C_a)\left[N\right]^T\left[N\right] d\Omega;$$

$$\left[C_4\right] = \int_\Omega -C_a\left[N\right]^T\left[N\right] d\Omega;$$

$$\left[K_1\right] = \int_\Omega a\left[B\right]^T\left[B\right] d\Omega;\left[K_2\right] = \int_\Omega b\left[B\right]^T\left[B\right] d\Omega;$$

$$\left[R_1\right] = \int_\Gamma \left[N\right]^T \alpha_w p_{en} d\Gamma;\left[R_2\right] = \int_\Gamma \left[N\right]^T \alpha_G T_{en} d\Gamma;$$

where $[N]$ is the column matrix of shape functions that relates pore pressure (temperature) field with their nodal values and $[B]$ relates the field of pore pressure (temperature) gradients and nodal values.

Equation 11 is solved using direct integration method based on the following assumption for the solution in the $(r+1)^{\text{th}}$ time step

$$\begin{aligned} \left\{p\right\}_{r+1} &= \left\{p\right\}_r + \Delta t\left(\left(1-\beta\right)\dot{p}_r + \beta\dot{p}_{r+1}\right) \\ \left\{\mathrm{T}\right\}_{r+1} &= \left\{\mathrm{T}\right\}_r + \Delta t\left(\left(1-\beta\right)\dot{\mathrm{T}}_r + \beta\dot{\mathrm{T}}_{r+1}\right) \end{aligned} \tag{12}$$

in which parameter β was set to $\beta = 1.0$ what yields to the unconditionally stable backward difference method that reads (Belytschko 2001):

$$\begin{aligned} &\left(\frac{\left[A\right]}{\Delta t} + \left[K_1\right]\right)\left\{p_{r+1}\right\} + \frac{\left[B\right]}{\Delta t}\left\{T_{r+1}\right\} = \\ &\qquad \frac{\left[A\right]}{\Delta t}\left\{p_r\right\} + \frac{\left[B\right]}{\Delta t}\left\{T_r\right\} + \left\{R_1\right\} \\ &\left(\frac{\left[C\right]}{\Delta t} + \left[K_2\right]\right)\left\{T_{r+1}\right\} + \frac{\left[D\right]}{\Delta t}\left\{p_{r+1}\right\} = \\ &\qquad \frac{\left[C\right]}{\Delta t}\left\{T_r\right\} + \frac{\left[D\right]}{\Delta t}\left\{p_r\right\} + \left\{R_2\right\} \end{aligned} \tag{13}$$

In Equation 13 the controlling parameters are coupled, therefore, for each time step the above set of linear equations have to be solved iteratively. As mentioned before, during the iteration process damage is assumed to be constant.

In the numerical analysis using finite elements the problem is relatively poor convergency. The reason is the transitional region of the state of the pore water from non-saturated to saturated, which is rather abrupt. To stabilize the numerical solution, time step must be relatively small. Moreover, in the finite element analysis one has to work with average finite element values of temperature, pore pressure and moisture.

4. NUMERICAL EXAMPLES

4.1 *Verification of the model*

To check the model and its implementation into the finite element code, the example taken from the literature (Bažant and Thonguthai 1978) is analyzed and the results are compared. In the example a concrete wall is heated from one side. Two different boundary conditions are considered (see Fig. 1). Calculated is distribution of temperature, pore pressure and moisture. The analysis is performed using 3D eight-node solid finite elements. The calculated distribution of pore pressure is plotted in Figure 1. The results are almost identical to those obtained by Bažant and Thonguthai (1978). This confirms that the model and its implementation are correct.

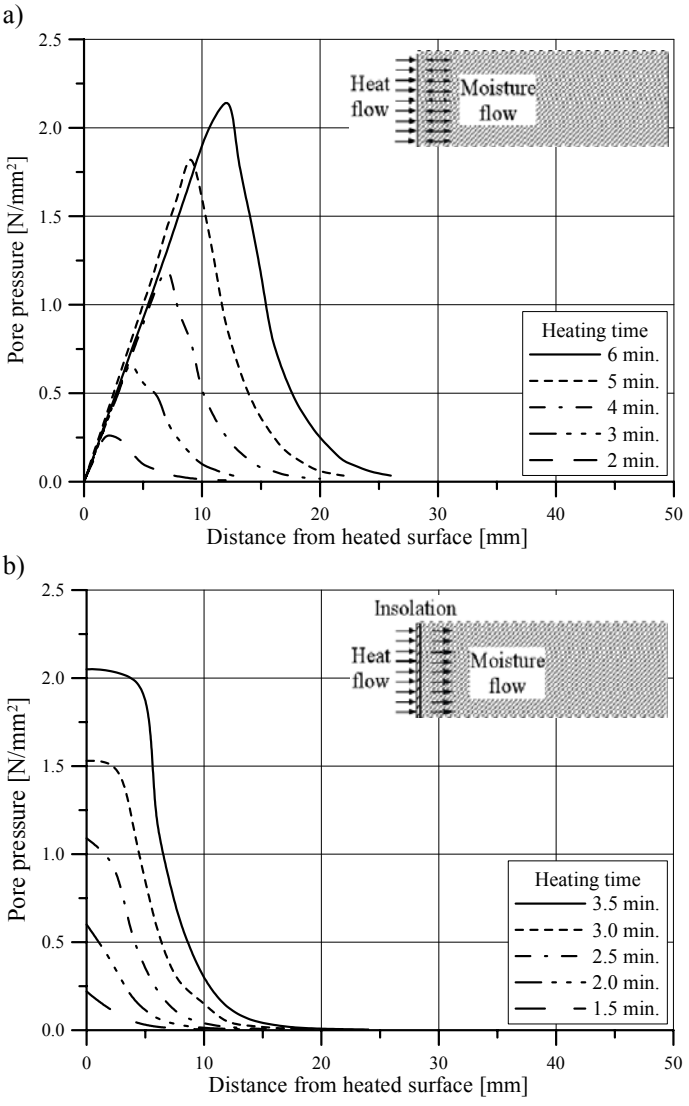

Figure 1. Calculated distribution of pore pressure for two different boundary conditions at the concrete surface.

4.2 *Spalling of concrete cover*

The preliminary numerical analysis of the problem of spalling of concrete cover is carried out. In the 3D FE analysis concrete slab was heated at the free surface (see Fig. 2). The height of the segment of the slab was $h = 100$ mm and the considered length of the slab was $l = 120$ mm (only symmetric part was analyzed). The linear increase of air temperature in time was assumed, with a temperature gradient of 80°C/min. Pore pressure at the surface was 1.0 kN/m^2. The analysis was carried out for time period of 12 minutes (duration of heating). The initial thermo-hygro and mechanical properties of concrete are summarized in Table 1.

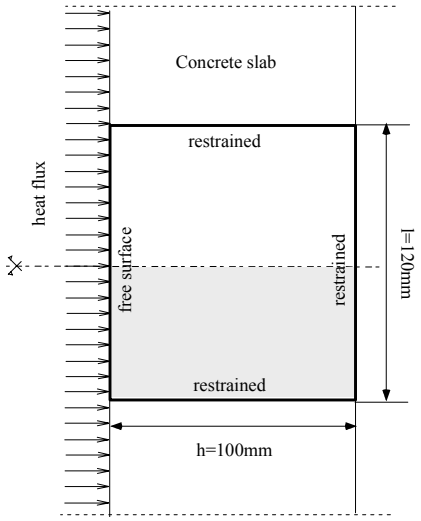

Figure 2. Geometry of the heated concrete slab.

In the mechanical part of the 3D FE analysis plane strain conditions were assumed. Except at the free concrete surface, all boundaries of the specimen were restrained in all three directions (see Figs 2 and 3). The co-rotational stress tensor for microplane model together with logarithmic strain tensor was employed. To obtain mesh objective results, crack band method was adopted (Bažant and Oh 1983). For the thermo-hygro-mechanical analysis the above discussed model was used, however, at current state of development, the complete coupling between thermo-hydro and mechanical part of the model was not yet implemented. Therefore, in the present example the influence of damage on the porosity was accounted for only in the mechanical part of the model based on Equation 10, i.e. calculation of pore pressure (moisture) and temperature distribution was not influenced by damage.

Table 1. Properties of concrete used in the FE analysis.

Young's modulus E [MPa]	28000
Poisson's ratio ν	0.18
Tensile strength f_t [MPa]	1.8
Uniaxial compressive strength f_c [MPa]	20.0
Fracture energy G_F [Nmm/mm^2]	0.08
Permeability a [m/s]	10^{-11}
Conductivity b [J/(msK)]	1.67
Heat capacity c [J/(kgK)]	900
Weight density ρ [kg/m^3]	2400

Water/cement ratio	0.5
Saturation water content [kg/m^3]	100
Surface emissivity of water α_w	max.
Surface emissivity of heat α_G	max.

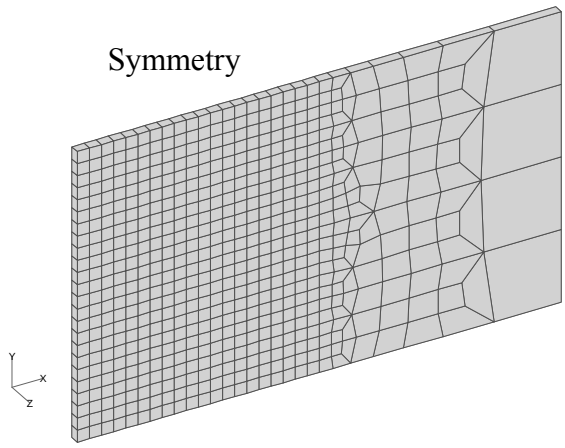

Figure 3 Finite element discretization.

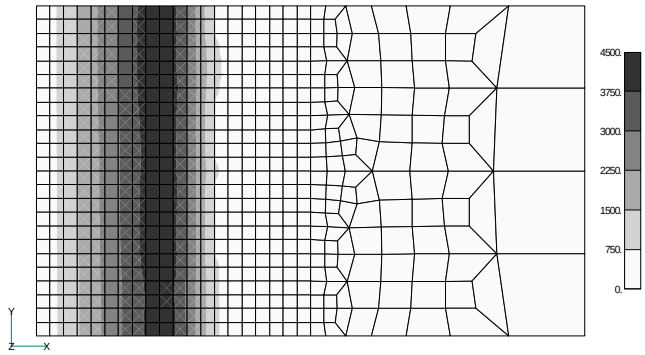

Figure 4. Distribution of pore pressure (in kN/m^2) at $t = 12$ min.

The distribution of pore pressure and temperature at $t = 12$ min. is shown in Figures 4 and 5, respectively. It can be seen that the maximum pore pressure reaches about 4.50 MPa and it is localized in the band parallel to the concrete surface. Its position is about 25 mm deep in concrete slab at place were concrete temperature is roughly 300^{0}C. Furthermore, the analysis shows that the position of maximal moisture approximately coincide with the maximal pore pressure.

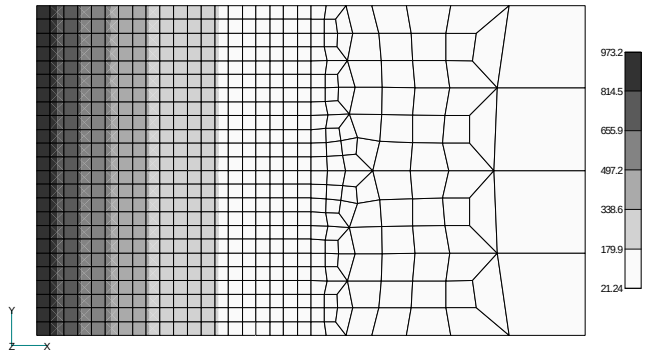

Figure 5. Distribution of temperature (in °C) at $t = 12$ min.

a)

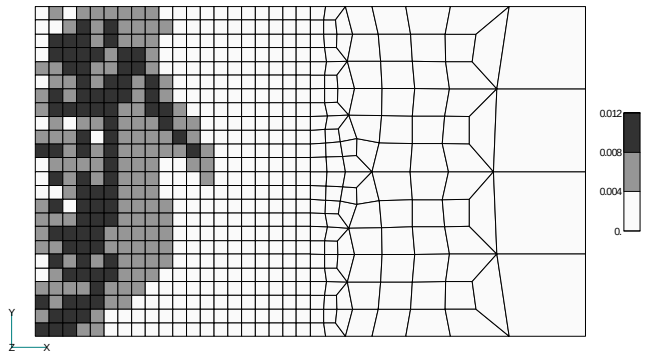

b)

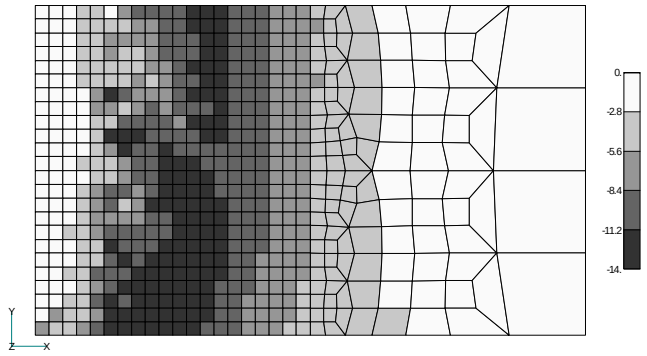

Figure 6. (a) Crack development (dark zones = maximum principal strains) at $t = 12$ min. and (b) Distribution of compressive stresses (in N/mm^2) at $t = 12$ min.

Figure 6 shows the distribution of maximal principal strains (Fig. 6a) and minimal principal stresses (Fig. 6b). Note that the strains shown in Figure 6a are calculated such that the non-elastic strains are subtracted from the total strain, i.e. only mechanical strain component is shown. From Figure 6a it can be seen that there is an indication of the formation of a vertical splitting crack (dark zones corresponds roughly to the crack width of 0.05 mm), which propagates almost parallel to the concrete surface at the depth of approximately 10 mm. At this position concrete temperature reaches about 600^{0}C, i.e. the resistance of concrete is

strongly reduced due to high temperature. Figure 6b shows the distribution of minimal principal stress (compression). Maximal values of compressive stress reaches about 17 MPa and it is close to the uniaxial compressive strength of concrete at $T = 20^0$C ($f_c = 20$ MPa). The position of the minimal stress approximately coincide with the position of maximal pore pressure, however, as can be seen from Figure 6a, the vertical splitting crack tends to form between concrete surface and position of maximal compressive stress.

The results of the analysis indicate that high compressive stresses, due to pore pressure and thermal induced stresses, together with geometrical instabilities (second-order effects) cause formation of vertical splitting crack (spalling of concrete cover). It is interesting that this effect was not observed in case when the geometrical instability was not taken into account (geometrically linear analysis). This can be seen from Figure 7, which shows the distribution of maximal principal strains (Fig. 7a) and minimal principal stresses (Fig. 7b) in case of geometrically linear analysis. As can be seen, the maximal principal strain at t = 12 min. is roughly 6 times smaller. Damage is localized close to the concrete surface. It is mainly due to direct temperature induced damage (degradation of strength and non-mechanical strains). The maximal compressive stress (approximately 14 MPa) is also smaller than in the geometrically nonlinear analysis.

a)

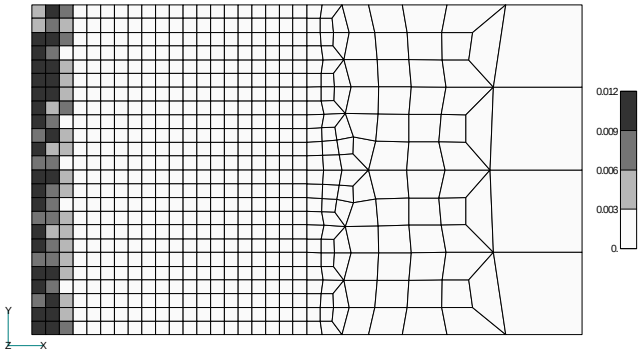

b)

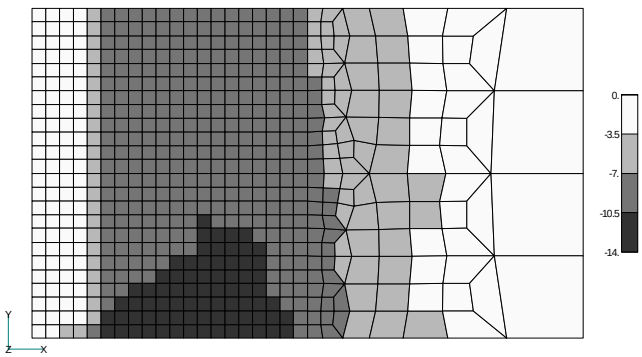

Figure 7. Geometrically linear analysis: (a) Crack development (dark zones = maximum principal strains) at $t = 12$ min. and (b) Distribution of compressive stresses (in N/mm^2) at $t = 12$ min.

The here presented results are only preliminary. To get more insight into the problem of spalling of concrete cover, further numerical studies have to be carried out in future.

5. CONCLUSIONS

In the present paper the thermo-hygro-mechanical model for concrete and its numerical implementation into the 3D finite element code are discussed. In the model the coupling between thermo-hydro and mechanical properties is considered in both directions. The model is formulated in the framework of continuum taking into account the basic principles of thermodynamic. It is pointed out that in the constitutive relationship the main difficulty is related to the identification of material parameters which are all coupled not only in the thermo-hygro part of the model, but also with the mechanical part of the model. The proposed model is implemented into the 3D finite element code. In the incremental iterative integration scheme the governing thermo-hydro and mechanical equations are solved simultaneously. The preliminary study of the problem of spalling of concrete cover indicates that the spalling is caused by the interaction between relatively high pore pressure and geometrically nonlinear effects (instability). The results show that the vertical crack parallel to the concrete surface forms between concrete surface and the position of the maximal pore pressure in concrete. Further improvement of the model and additional numerical studies are needed to clarify the problem of spallling of concrete cover in more detail.

REFERENCES

Bažant, Z.P. and Thonguthai, W. 1978. Pore pressure and drying concrete at high temperature. *ASCE Journal of the Engineering Mechanics Division*, Vol. 104, No. EM5, 1059- 1079.

Bažant, Z. P. and Oh, B. H. 1983. Crack band theory for fracture of concrete. *RILEM* 93(16): 155-177.

Bažant, Z.P. and Kaplan, M.F. 1996. *Concrete at High Temperatures: Material Properties and Mathematical Models*. Harlow, Longman.

Bažant, Z.P. and Cusatis, G. 2005. *Concrete creep at high temperature and its interaction with fracture: recent progress*. CONCREEP-7, Ed. Pijaudier-Cabot, Gerard & Acker, Hermes Science, 449-460.

Belytschko T., Liu W.K. and Moran, M. 2001. *Nonlinear Finite Elements for Continua and Structures*. John Wiley & Sons Ltd.

Gawin, D., Majorana, C.E. and Schrefler, B.A. 1999. Numerical Analisys of hygro-thermal behaviour and

damage of concrete at high temperatures. *Mech. Cohes.-Frict. Mater.* **4**(1), 37-74.

Harmathy, T.Z., and Allen, L.W. 1973. Thermal properties of selected masonary unit concretes. *Journal of American Institute*, Vol. 70, 132-144.

Khoury, G.A.,Grainger, B.N. and Sullivan, P.J.E. 1985a. Transient thermal strain of concrete: literature review, conditions within specimens and behaviour of individual constituents. *Mag. of Conc. Res.* **37**(132), 131-144.

Ožbolt, J., Li, Y.-J. and Kožar, I. 2001. Microplane model for concrete with relaxed kinematic constraint. *International Journal of Solids and Structures* 38: 2683-2711.

Ožbolt, J., Kožar, I., Eligehausen, R., and Periškić, G. 2005. Three-dimensional FE analysis of headed stud anchors exposed to fire. *Computers and Concrete* Vol. 2, No. 4, 249-266.

Pearce, C.J., Bićanić, N. and Nielsen, C.V. 2003. *A transient thermal creep model for concrete*. Computational Modeling of Concrete Structures, Sweets & Zeitlinger, Lisse.

Schneider, U. 1986. *Properties of Materials at High Temperatures, Concrete*. 2nd. Edition, RILEM Technical Comitee 44-PHT, Technical University of Kassel, Kassel.

Schneider, U. 1988. Concrete at High Temperatures – A General Review. *Fire Safety Journal* 13(1), 55-68

Stabler, J. 2000. *Computational modelling of thermomechanical damage and plasticity in concrete*. PhD thesis, The University of Queensland, Brisbane.

Terro, M.J. 1998. Numerical modelling of the behaviour of concrete structures in fire. *ACI Struct. Journal* 95(2), 183-193.

Thelandersson, S. 1983. On the multiaxial behaviour of concrete exposed to high temperature. *Nucl. Eng. and Design* 75(2), 271-282.

Thelandersson, S. 1987. Modelling of combined thermal and mechanical action in concrete. *J. of Eng. Mech*. 113(6), 893-906.